Available online at www.sciencedirect.com
ScienceDirect
Diamond & Related Materials 15 (2006) 1622–1628
DIAMOND AND RELATED MATERIALS
www.elsevier.com/locate/diamond

Growth of mechanically fixed and isolated vertically aligned carbon nanotubes and nanofibers by DC plasma-enhanced hot filament chemical vapor deposition

H.Y. Yap [a], B. Ramaker [b], A.V. Sumant [c], R.W. Carpick [c,*]

[a] Department of Physics, University of Wisconsin-Madison, United States
[b] Department of Chemistry, University of Wisconsin-Madison, United States
[c] Department of Engineering Physics, University of Wisconsin-Madison, United States

Received 1 August 2005; received in revised form 21 January 2006; accepted 23 January 2006
Available online 6 March 2006

Abstract

Vertically aligned, mechanically isolated, multiwalled carbon nanotubes (MWCNTs) and nanofibers (MWCNFs) were grown using an array of catalyst nickel nanowires embedded in an anodic aluminum oxide (AAO) nanopore template using DC plasma-enhanced hot filament chemical vapor deposition (HFCVD). The nickel nanowire array, prepared by electrodeposition of nickel into the pores of a commercially available AAO membrane, acts as a template for CNT and CNF growth. It also provides both a mechanical "fixed support" boundary condition and enforces sufficient spatial separation of the CNT/CNFs from each other to enable reliable and well-controlled mechanical testing of individual vertically aligned CNT/CNFs. In contrast with other AAO-templated growth methods, no post-growth etching of the AAO is required, since the CNTs/CNFs grow out of the pores and remain vertically aligned. A mixture of hydrogen and methane was used for the growth, with hydrogen acting as a dilution and source gas for the DC plasma, and methane as the carbon source. A negative bias was applied to the sample mount to generate the DC plasma. The filaments provided the necessary heat for dissociation of molecular species, and also heat the sample itself significantly. Both of these effects assist the CNT/CNF growth. Minimal heating came from the low-power plasma. However, the associated DC field was essential for the vertical alignment of the CNTs and CNFs. Scanning electron, transmission electron, and atomic force microscopy confirm that the CNT/CNFs are composed of graphitic layers, and form a vertically aligned, relatively uniform, and dense array across the AAO template. A significant number of the structures grown are indeed high quality nanotubes, as opposed to more defective nanofibers that are often predominant in other growth methods. This method has the advantage of being scalable and consuming less power than other techniques that grow vertically aligned CNTs/CNFs.

1. Introduction

The spectacular proliferation of techniques for growing nanostructured materials continues to enable new scientific research and applications. Carbon nanotubes (CNTs) and nanofibers (CNFs) are of particular interest because of their remarkable mechanical, electronic, and chemical properties [1]. For most electronic applications of CNT/CNFs, such as the cold cathodes in field-emission flat panel displays and nanotransistors [2–4], an ordered and dense array of vertically aligned nanotubes over a large area is required. This is also desirable for testing the mechanical properties of CNT/CNFs, or the design of layered and aligned CNT/CNF composites. One method of achieving this alignment is by the use of anodic aluminum oxide (AAO) pore arrays. The AAO arrays consist of deep, vertically aligned pores as small as 20 nm in diameter, and are thus ideal as templates for CNT/CNF growth. Furthermore, the pores can create a "fixed" mechanical boundary condition for the CNT/CNFs, and provide separation between CNTs that otherwise tend to grow as dense "carpet" of filaments, with significant lateral van der Waals interactions between them [1]. Such separation facilitates nanomechanical testing such as compression and bending tests, of individual tubes.

* Corresponding author. Tel.: +1 608 263 4891; fax: +1 608 263 7451.
E-mail address: carpick@engr.wisc.edu (R.W. Carpick).

0925-9635/$ - see front matter © 2006 Elsevier B.V. All rights reserved.
doi:10.1016/j.diamond.2006.01.014

Several investigations have already utilized an AAO-pore template to grow CNT/CNFs via thermal chemical vapor deposition (CVD) [5,6]. However, the CNT/CNFs grown by this method are not vertically aligned or isolated once growth extends past the pores by an appreciable amount. Thus, thermal CVD yields only a matted, entangled mass of CNT/CNFs above the template surface. To correct this, ultrasonic treatment [7] or dry etching methods such as ion milling or reactive ion etching [8] are used to remove the topmost layer of CNT/CNFs and other carbonaceous material, leaving aligned CNT/CNFs within the channels of the AAO pores. Wet etching, for example with phosphoric acid [7,8], is used to remove an appropriate portion of the AAO template to expose freestanding CNT/CNFs.

Plasma-enhanced CVD yields more consistent vertical alignment compared to thermal CVD. Some investigations have employed IC-(inductively coupled) [9] and ECR-(electron cyclotron resonance) [10–12] microwave plasma-enhanced CVD to successfully grow vertically aligned CNT/CNFs from the pores of AAO templates. These methods have the catalyst in the pores [9–12] or can be catalyst-free [13]. Indeed, these methods provide good mechanical anchoring of the CNT/CNFs. However, high frequency plasma generation requires rather complex setups and larger power consumption than DC plasma-enhanced CVD. For example, in Ref. [10], 700 W of power was needed.

DC plasma-enhanced hot filament CVD (HFCVD) is a simpler, low-power, and scalable growth methodology. HFCVD was first used by Ren et al. [14] to grow well-aligned CNT/CNFs on a Ni-coated glass substrate. Subsequently, Cruden et al. [15] used DC plasma-enhanced HFCVD to grow aligned CNT/CNFs on Ni-coated silicon (Si). These Ni-coatings require thermal or chemical processing to break them up into nanoscale islands before growth to properly function as CNT/CNF catalysts. Furthermore, the anchoring of the islands to the substrate is not designed to be mechanically robust. CNT/CNFs were grown in the pores of an AAO template using DC plasma-enhanced CVD by Kim et al. [16], but the CNT/CNFs only grew on the surface between, rather than in, the pores. Later, this group did accomplish some CNT/CNF growth out of the AAO pores, but they were still curled [17].

Our goal was to grow mechanically isolated, vertically aligned CNT/CNFs with well-defined "fixed" mechanical boundary conditions, without the need for high power consumption or post-growth etching of the membrane. This was accomplished by combining, for the first time, DC plasma-enhanced HFCVD with catalyst-containing AAO pore membranes.

2. Experimental

60-μm-thick *Whatman Anodisc 25* AAO filter membranes were used. The membrane has pores ~200 nm in diameter, with a center-to-center spacing ranging from 300–400 nm, and the membrane is 40–60 μm thick. No anodization or pore-widening was performed, saving a considerable amount of time in the sample preparation stage. The backside of the filter membrane was coated with an approximately 180-nm-thick layer of silver or gold using a *Denton Vacuum Desk II* ion sputterer. This metallic backing was needed for electrodeposition of nickel into the pores, and further acted as a structural support for the brittle AAO membrane. $NiSO_4 \cdot 6H_2O$ solution from *Technic, Inc.* was used for electrodeposition, and the power source was a 1.5 V AA battery. The electrodeposition time was approximately 70 min, at which time overdeposition could be observed at the outer rings of the circular membrane.

CNT/CNF growth was then carried out in a custom-built DC plasma-enhanced HFCVD chamber (Fig. 1) which has a base pressure of 4×10^{-3} Torr. Heating was accomplished with two 0.020-in.-diameter tungsten filaments (E), all approximately 60 mm in length with a separation distance of 5 mm between each filament. Two filament supports (E) were suspended above the sample mounting stage by copper rods (C) and (C′) electrically isolated from the chamber. These two rods served as the terminals for the filament circuit (powered by a DC power supply (A)) and in addition, also acted as the anode for the DC plasma (G). A 35-mm-diameter circular stainless steel disk sat atop an adjustable, electrically isolated steel post-inserted into the bottom the chamber. To electrically isolate the stage from the plasma, a ceramic spacer similar in size to the steel disk was used. Set on top of the spacer was a stainless steel sample mount (F) acting as the cathode for the plasma circuit. The sample was affixed to a silicon wafer die by silver colloidal paste (D) and the wafer die itself was affixed to the plasma cathode (F) again by silver paste. The distance from the filaments to the sample was approximately 10 mm. The temperatures of the Si dies (D), filaments (E) and sample mount (F) were monitored by an optical-sighting pyrometer. The chamber is linked to a vacuum pump via hoses (I).

Whenever new tungsten filaments were installed, a methane pretreatment was performed. With 10 sccm methane at 10–20 Torr, the filaments were heated to approximately 1500 °C for 10 min, then at 1800–1900 °C for 5 min and finally for a brief

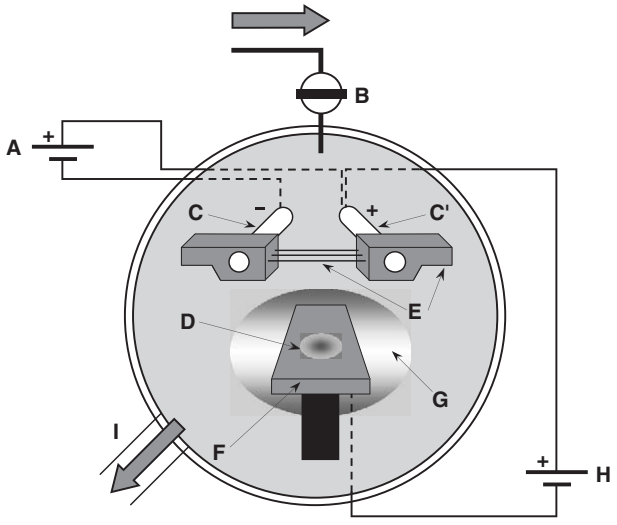

Fig. 1. Schematic diagram of the HFCVD chamber. (A) power supply for heating of filaments via copper rods, (B) combined gas feed line leading to chamber, (C and C') copper rod electrodes (also acting as plasma anode), (D) sample on a small Si die, (E) W filaments and supports, (F) sample mount (plasma cathode), (G) plasma, (H) DC power supply for the plasma, (I) hoses to vacuum pump.

moment at 2100 °C to form a thin tungsten carbide layer, which prevents tungsten evaporation during subsequent CNT/CNF growth. This pretreatment also prevented tungsten contamination of the sample, which poisons the nickel catalyst and prevents CNT/CNF growth. As expected, there was no sign of W contamination on any samples as verified by X-ray photoemission spectroscopy.

Hydrogen was then introduced at 40 sccm via a feed line (B). The temperature of the sample/Si wafer piece (D) was slowly increased to approximately 600 °C by filament heating. After both pressure and temperature stabilization, DC plasma (G) was activated by a DC power supply (H) at a bias voltage of 455 V. A visible glow discharge enveloped the region surrounding the portion of the cathode above the ceramic spacer, producing an ion current of ~100 mA, corresponding to a power input of 45.5 W. Upon plasma activation, the filaments were at a temperature of approximately 1800 °C. Methane was then introduced at 8 sccm, thus keeping the ratio of hydrogen to methane at 5 : 1. An operating pressure of approximately 10 Torr was used for growth. All gas flows are controlled by MKS 2259 mass flow controllers. The growth time of 25 min gave CNT/CNF lengths of 1–2 μm. Longer growth times are also possible. The sample temperature during growth was approximately 760 °C.

The structure and morphology of the CNT/CNFs were studied using a LEO 1530 high resolution/low voltage scanning electron microscope (SEM), a Digital Instruments (DI) Nanoscope IV atomic force microscope (AFM), a JEOL 200 CX-II transmission electron microscope (TEM) with electron diffraction capabilities, and a Philips CM200UT high resolution transmission electron microscope (HRTEM).

3. Results and discussions

Fig. 2A is a SEM aerial view of the pore structure of the AAO membrane before electrodeposition of the Ni. The pores have the typical degree of order and are well-spaced apart. Fig. 2B is a SEM aerial view of the AAO pores after undergoing Ni electrodeposition at the boundary of a region of overdeposition. Some pores were overdeposited with Ni at the sides (labeled A in Fig. 2B), while other pores had either Ni deposition significantly below the template surface or no deposition at all (labeled B). However, in most cases, the deposited Ni nanowires were close to but just below the open ends of the pores (labeled C). These could be found over large areas of the AAO membrane. These areas were then cut from the membrane and used for CNT/CNF growth in the chamber. Fig. 2C is a cross-sectional SEM view of the AAO pores filled with Ni. The dark line across Fig. 2C denotes the boundary between an unfilled region (i) and a Ni filled region (ii).We typically deposited the Ni nanowires so as to nearly completely fill the pores. The nanowire growth is rather non-uniform in our case because we have not performed any etching to open up the pores on the bottom side of the membrane. On this bottom side, the pores are branched and have varying diameters, thus leading to significant variations in the subsequent height of the deposited nanowires. This can be easily remedied, as shown in more detail by Lee and Suh [18].

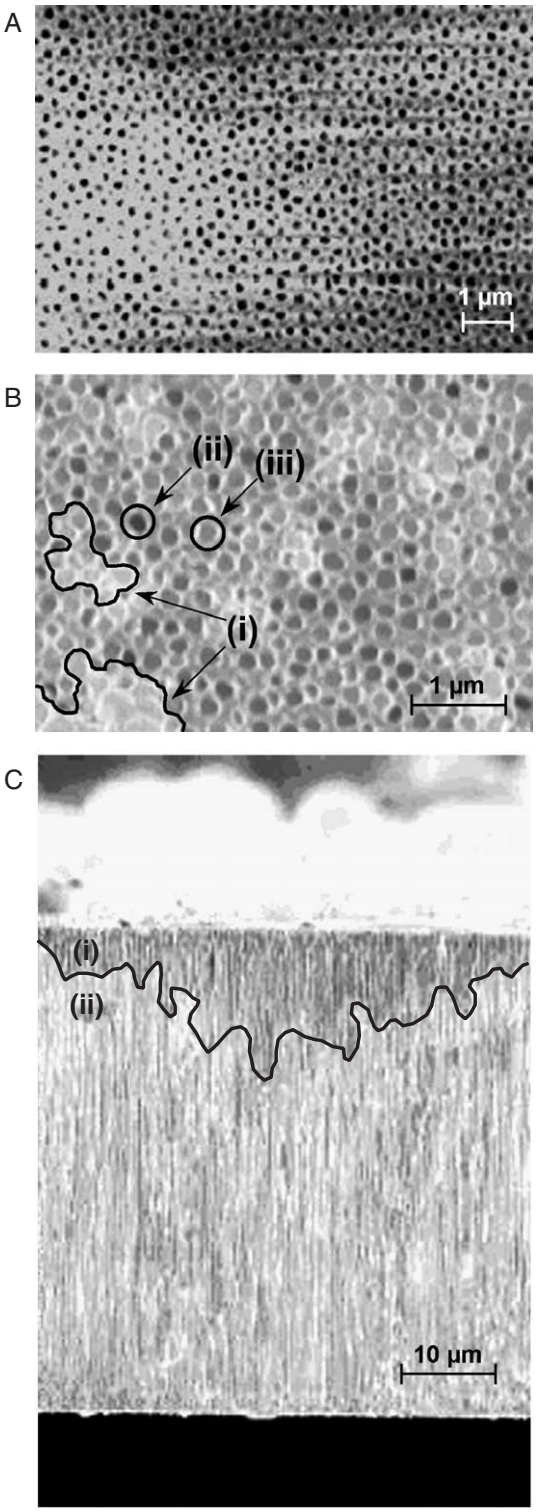

Fig. 2. (A) SEM image of the 2D array of pores of an AAO membrane before electrodeposition of the Ni catalyst. (B) Section of the AAO membrane near a boundary of overdeposition. (i) overdeposited pores where nickel has overflowed out of the pore. (ii) catalyst is significantly below the top of the membrane. (iii) likely pores for successful CNT/CNF growth due to intermediate nickel deposition (not overdeposited, i.e. bright, nor underdeposited, i.e. dark. (C) Cross-sectional view of the AAO membrane after deposition of nickel. Note the contrast between the top-portion of the pores with the rest of template. (i): non-deposited sections of the pores. (ii): brighter, deposited section of the pores.

Thermal CVD and HFCVD without bias were attempted first but these resulted in CNT/CNF growth with no vertical alignment. Fig. 3A shows a series of SEM top views of CNT/CNFs produced by DC plasma enhanced HFCVD. Clearly, they extend directly out of the AAO pores. This particular region was intentionally scratched using an AFM tip to remove some of the CNT/CNFs and expose the AAO's porous surface for imaging. Fig. 3B is a SEM image of a region of the sample tilted at 45° which illustrates the high degree of vertical alignment of the CNT/CNFs. No entanglement was apparent. The diameters of the CNT/CNFs range from 70–200 nm. Unlike other methods of vertical alignment, our CNT/CNFs are not closely packed at

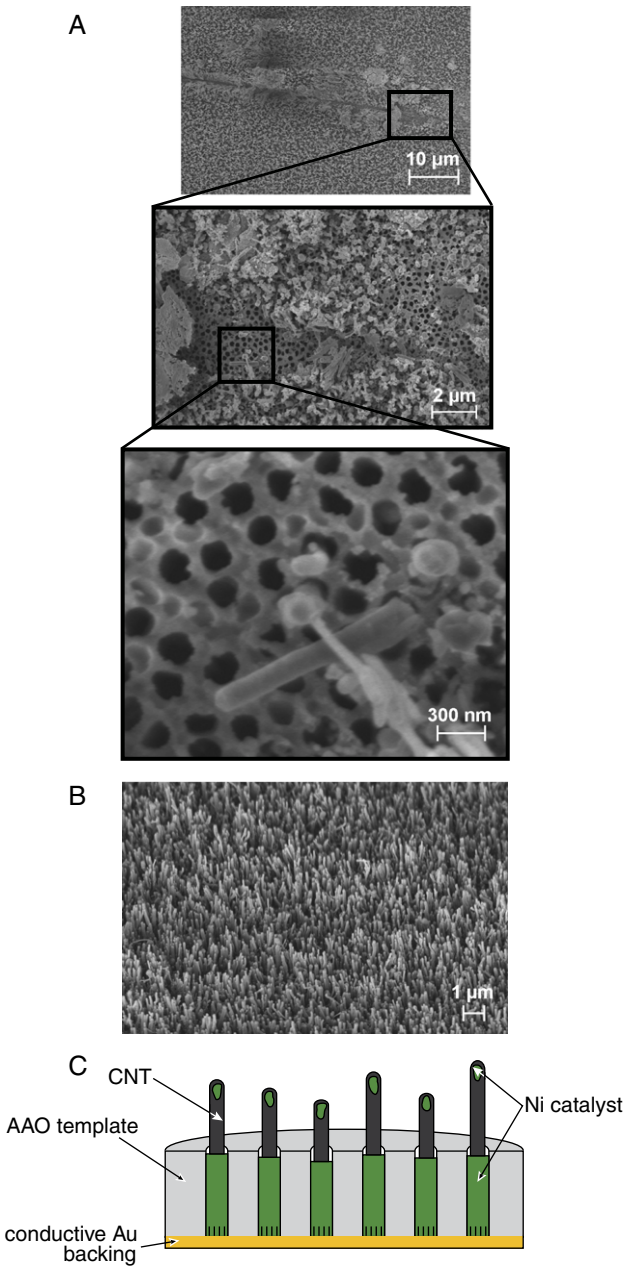

Fig. 3. (A) SEM aerial views of CNT/CNFs emerging from the pores, from a region partially exposed by scraping CNT/CNFs away. (B) SEM image of the sample acquired at 45°. (C) Schematic of the cross-sectional view of the whole sample.

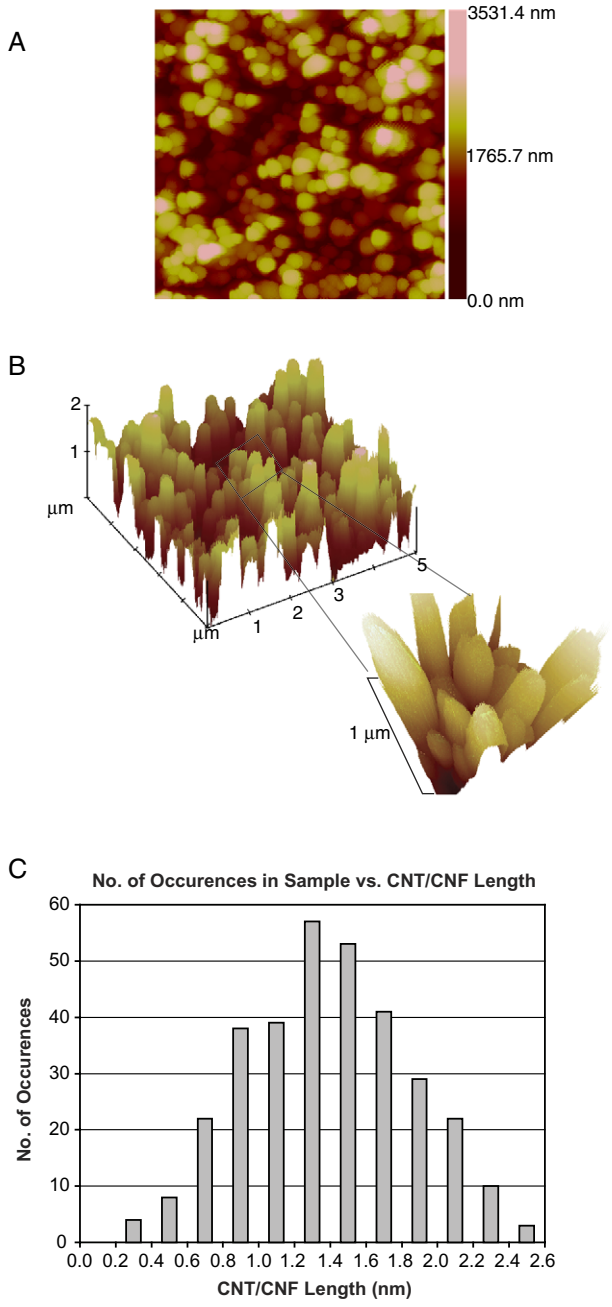

Fig. 4. (A) AFM image of a $5\times5\,\mu m^2$ area of the CNT/CNF sample. (B) 3D AFM rendering of the same area. Inset: $1\times1\,\mu m^2$ close-up of a portion of this image. (C) Histogram of the heights of the CNT/CNFs grown in the area shown in (A).

their van der Waals spacing. While some CNT/CNFs are slightly bent and touching their neighbors, the vast majority are separated from all of their neighbors by gaps as large as ~100 nm, meaning that they are mechanically isolated from their neighbors. Fig. 3C is a schematic of the cross-sectional view of the final sample.

One concern in plasma-based growth techniques, particularly high density DC plasmas, is damage in the form of ion bombardment. No such damage from our low power DC plasma was evident from any of the imaging we performed.

Using high aspect ratio "STING" probes from Mikromasch (type DP16/STING/Al BS), topographical images of the aligned CNT/CNFs were collected in intermittent contact mode AFM at a scan rate of 1 Hz. Fig. 4A is a topographic AFM image of a typical $5 \times 5\,\mu m^2$ portion of the sample. Fig. 4B is a three-dimensional rendition of Fig. 4A to better illustrate the height profile of the sample. The inset to Fig. 4B shows the CNT/CNFs at higher magnification. Separation between many of the CNT/CNFs is again apparent. Some of the structures appear to be touching. However, in AFM, the finite size of the tip makes vertical features appear wider than their true size and correspondingly can fail to detect gaps between closely spaced high-aspect ratio structures. Fig. 4C is a histogram of the heights of the CNT/CNFs from this image. The mode of the height distribution of these CNT/CNFs was approximately 1.2–1.4 μm. The distribution was rather wide, but a considerable amount of the CNT/CNFs exceeded 1 μm in height, which is suitable for mechanical testing such as axial compression and buckling experiments.

To further characterize the CNT/CNFs' structure, TEM and HRTEM studies were conducted. Fig. 5A shows a TEM micrograph at a magnification of 340,000×. Different structures are observed. On the left is a CNT/CNF with defective, herringbone-like internal structures [15]. On the right, the CNT/CNF has a hollow structure in the core. The Ni catalyst sits on top of the CNT/CNFs in the shape of a cone with smoothed edges, consistent with the high temperature "tip growth" model. The sides of these cones become more parallel to the tube axis as one goes deeper into the tube. As such, the graphitic walls are also almost parallel to the tube axis. Catalytic cones instead of spheres form at the tips because of the lower free energy of the catalyst–carbon interface compared with the catalyst–vacuum interface. The quality and morphology of structures grown here surpasses that in Refs. [16,17] using DC plasma-enhanced CVD and AAO pores, where the morphology of CNT/CNFs grown resembled more of a cone shape. An electron diffraction pattern of a CNT/CNF's walls obtained from TEM is shown in Fig. 5B. The brightest innermost ring circling the intensely bright central beam represents the diffraction pattern of the (002) graphite plane. Two opposite regions or arcs of the ring are bright,

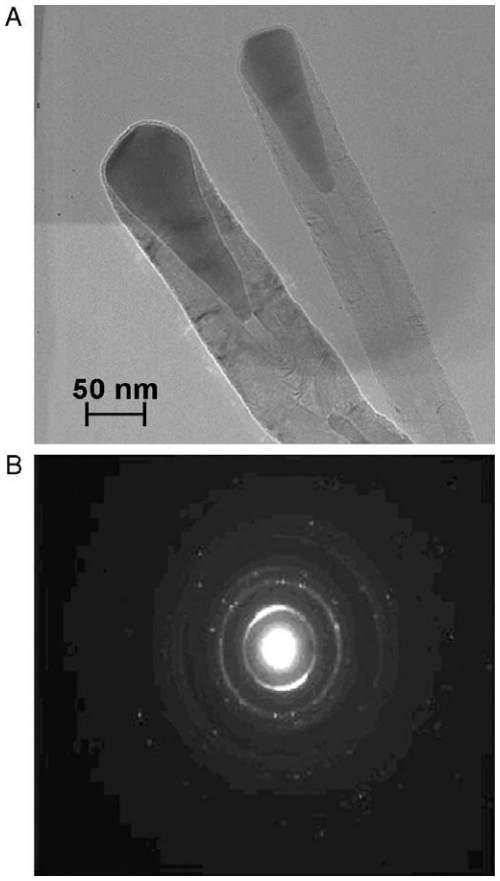

Fig. 5. (A) TEM image of a CNT. At right: a CNT, with a hollow interior free of defects. At left: a CNF, with a partially defective herringbone interior. (B) Electron diffraction pattern of the graphene walls of a CNT illustrating the high degree of ordering of the planes.

indicating a significant degree of orientation. Also, (101), (102) and (110) diffraction rings are present. The ring patterns indicate that the CNT/CNF here is indeed largely graphitic in nature, and not made of disordered carbon.

To precisely determine whether these tubular structures are CNFs or CNTs, their graphitic walls are observed in more detail with HRTEM. If there is a non-zero angle between the

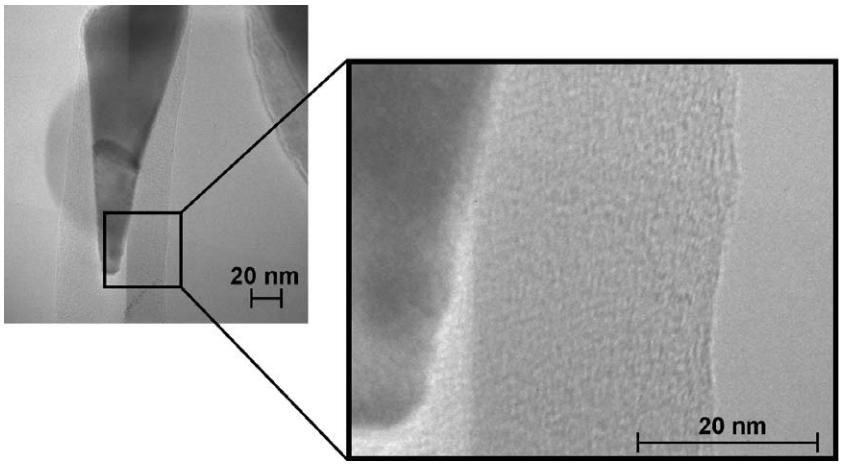

Fig. 6. HRTEM image of a CNT including a magnified view of the right wall's structure. The graphene planes run parallel to the tube axis.

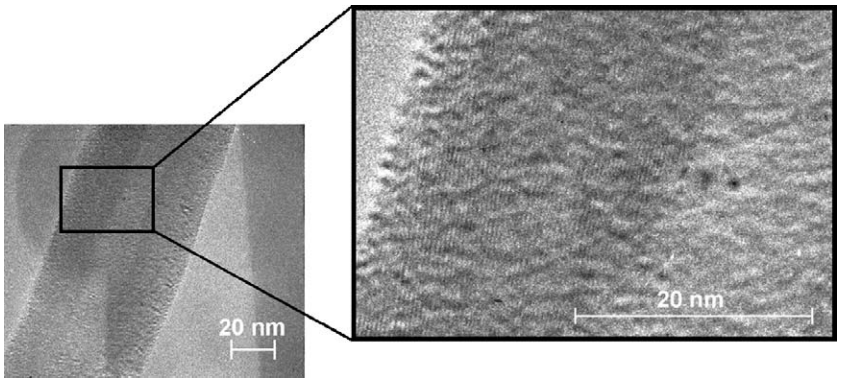

Fig. 7. HRTEM image of a CNF including a magnified view of the left wall's structure. The graphene planes run at a small angle to the tube axis.

inclination of the walls and the tubular axis, one would classify these structures as CNFs instead of CNTs [19]. Our results show that we grew a mixture of both. Fig. 6 shows the HRTEM images of what we characterize as a CNT. On the right wall structure of Fig. 6, the graphitic planes can be seen to be parallel to the tube axis as opposed to the sides of the Ni catalyst particle. They extend all along the length of the CNT. There are 80–90 graphene shells in this CNT, corresponding to an outer radius of approximately 43 nm and an inner radius of 10 nm. However, in Fig. 7, there is a finite angle between the tube axis (or its boundary) and the inclination of planes of the walls, and so the structure is more aptly classified as a CNF. There are 60–70 graphene shells in this CNF, corresponding to an outer radius of approximately 35 nm and an inner radius of 10 nm. Overall, both defective carbon nanofibers and less defective (and possibly defect-free) carbon nanotubes were observed in the TEM and HRTEM. This is an improvement over most other growth methods of vertically aligned CNT/CNFs in DC plasma-enhanced CVD, which overwhelmingly exhibit the defective herringbone or "bamboo-like" interior structures characteristic of CNFs [15]. Detailed TEM and EELS studies to quantify the CNT vs. CNF statistics for our samples are under way.

The mechanism of CNT/CNF growth in AAO pores is still unclear. Lee et al. [20] have claimed that the AAO itself plays a role as a catalyst in promoting the growth of CNT/CNFs on their surface. For our samples, SEM images indicate that the pores do not always perfectly circumscribe the CNT/CNFs. Thus, we believe that the AAO played little or no role as a catalyst. Also, with an increase in growth time, the length of the tubes increased correspondingly. In the AAO catalyst-driven growth described by Lee et al., the tubes become thicker but remain embedded within the pores.

The low plasma power here contributed little to substrate heating as compared with the heat originating from the filaments and subsequently conducted through the gases. The increase in temperature when the plasma was turned on with no hot filament was only ~150 °C. This corresponds well with simulations performed in [21]. The roles of the filaments in dissociating hydrogen and possibly methane, as well as exciting or ionizing hydrogen and methane species, might not be negligible as claimed in Refs. [15,21]. It is also possible that the plasma, although low in power, assists the growth kinetics by helping to dissociate methane, enhancing the population of reactive C atomic species. Further investigations of the role of the hot filaments in the plasma chemistry and synthesis of CNT/CNFs are being conducted.

Fig. 8 illustrates the advantageous nature of the anchoring at the bottom inside the pores. AFM was used to find an isolated CNT/CNF and compress it axially with the silicon tip of a stiff AFM cantilever with a force constant of 43 N/m, as determined experimentally using the Sader method [22]. The inset of Fig. 8 illustrates the experimental set up of the AFM cantilever-CNT/CNF system. The loading phase consists of an initial out-of-contact portion, a linear increase in force when the CNT/CNF comes into contact with tip and remains upright (and only elastic axial compression occurs), a sudden drop in force (due, we believe, to buckling of the tube), a plateau in the force (due to continued buckling of the tube) and finally a rapid increase (as the buckled CNT/CNF is deformed so much that it now poses resistance to further compression). Note that the force

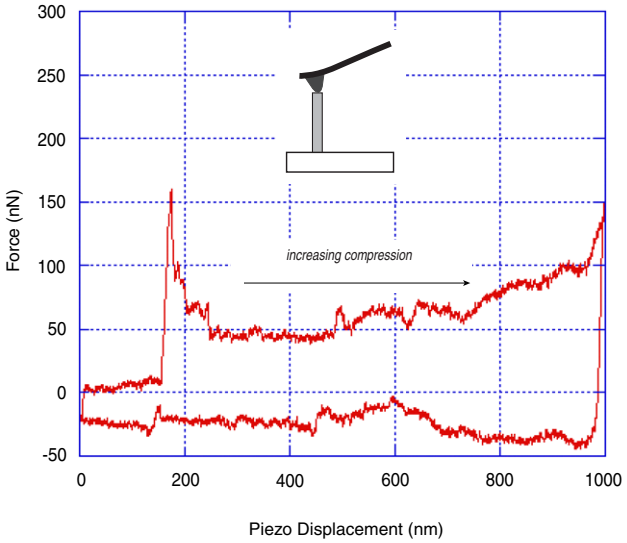

Fig. 8. Plot of force versus sample displacement of an individual CNT/CNF being axially compressed by a stiff AFM cantilever. The arrow indicates an instability during compression that we attribute to buckling. The upper curve is where compression is increased while the lower curve is where decompression occurs. Inset: Geometry of compression tests performed by the AFM cantilever on the individual CNT/CNF.

drop corresponds to a phase of negative stiffness, which has potentially interesting consequences for the design of composites [23,24]. The large hysteresis between the loading and unloading (f) curves (also seen in Refs. [7,9]) indicates adhesive forces at work between the CNT/CNF and the substrate/template or even between the outermost walls of the CNT/CNF if it is severely buckled over itself. The loading and unloading cycles are repeatable to a high degree at low frequencies, i.e. 1–2 Hz, indicating that the CNT/CNF has not been permanently damaged. Accurate positioning of the tip above the CNT/CNF is necessary for this negative stiffness to be observed. These loading tests are very sensitive to the initial loading conditions. More detailed studies of these phenomena will be discussed separately [25].

4. Summary

DC plasma-enhanced HFCVD was used to grow vertically aligned, mechanically fixed and isolated MWCNTs and CNFs out of AAO pores. The commercial AAO pore template was sufficient for growth as provided, once Ni nanowire catalysts were electrochemically deposited into the pores, i.e. no additional anodization or pore widening was required. Unlike with thermal CVD methods, no wet or dry etching of the AAO template after CNT/CNF growth was needed to expose the CNT/CNFs. Also, no pretreatment was needed to break the metal catalyst up into nanoparticles. The DC electric field applied to create the plasma also provides the necessary driving force to vertically align the CNT/CNFs. The CNT/CNFs grow in the "tip growth" mode, and a significant proportion of the structures grown were actually high-quality nanotubes with completely hollow inner cores, not defective nanofibers. The power input required is low compared to microwave plasma-enhanced CVD. The use of hot filaments assists the growth kinetics by heating the substrate as well as dissociating the growth species. Individual CNT/CNFs exhibit a significant degree of mechanical robustness as evidenced by reproducible nano-scale compression experiments with AFM, indicating strong anchoring of the CNT/CNF to the substrate and opening up opportunities for extensive nanomechanical testing.

A recent article, "On the role of activation mode in the plasma - and hot filaments-enhanced catalytic chemical vapour deposition of vertically aligned carbon nanotubes" by C.S. Cojocaru and F. Le Normand (Thin Solid Films, in press, corrected proof), also showed that the hot filament is crucial in producing highly reactive radicals, which in turn prevent the coverage of carbon over the catalyst and substrate. The role of the hot filament in producing reactive radicals cannot be underestimated as suggested by authors of Refs. [15] and [21] of this paper.

Acknowledgements

The authors acknowledge the financial support of NSF under grant #CMS-0136986. We thank Alex Kvit for expert assistance with the TEM, Anne Bentley for assistance with the electrodeposition process, and R.S. Lakes for useful discussions.

References

[1] M.S. Dresselhaus, H.J. Dai, MRS Bull. 29 (2004) 237 (and references therein).
[2] S. Iijima, T. Ichihashi, Nature (Lond.) 363 (1993) 603.
[3] W.A. de Heer, A. Chatelain, D. Ugarte, Science 270 (1995) 1179.
[4] W.B. Choi, J.U. Chu, K.S. Jeong, E.J. Bae, J.W. Lee, J.J. Kim, J.O. Lee, Appl. Phys. Lett. 79 (2001) 3696.
[5] T. Kyotani, L. Tsai, A. Tomita, Chem. Mater. 8 (1996) 2109.
[6] T. Iwasaki, T. Motoi, T. Den, Appl. Phys. Lett. 75 (1999) 2044.
[7] J. Xu, X. Zhang, F. Chen, T. Li, Y. Li, X. Tao, Y. Wang, X. Wu, Appl. Surf. Sci. 239 (2005) 320.
[8] A. Yin, H. Chik, J. Xu, IEEE Trans. Nanotech. 3 (2004) 147.
[9] J.H. Yen, I.C. Leu, M.T. Wu, C.C. Lin, M.H. Hon, Electrochem. Solid-State Lett. 7 (2004) H29.
[10] P.L. Chen, J.K. Chang, C.T. Kuo, F.M. Pan, Diamond Relat. Mater. 13 (2004) 1949.
[11] P.L. Chen, J.K. Chang, C.T. Kuo, F.M. Pan, Appl. Phys. Lett. 86 (2005) 123111.
[12] P.L. Chen, J.K. Chang, F.M. Pan, C.T. Kuo, Diamond Relat. Mater. 14 (2005) 804.
[13] B.A. Yao, N. Wang, T. Kuo, J. Phys. Chem., B 105 (2001) 11395.
[14] Z.F. Ren, Z.P. Huang, J.W. Xu, J.H. Wang, P. Bush, M.P. Siegal, P.N. Provencio, Science 278 (1998) 100.
[15] B.A. Cruden, A.M. Cassell, Q. Ye, M. Meyyappan, J. Appl. Phys. 94 (2003) 4070.
[16] M.J. Kim, J.H. Choi, J.B. Park, S.K. Kim, J.B. Yoo, C.Y. Park, Thin Solid Films 435 (2003) 312.
[17] M.J. Kim, T.Y. Lee, J.H. Choi, J.B. Park, J.S. Lee, S.K. Kim, J.B. Yoo, C.Y. Park, Diamond Relat. Mater. 12 (2003) 870.
[18] J.S. Lee, J.S. Suh, J. Appl. Phys. 92 (2002) 7519.
[19] D. Nolan, D.C. Lynch, A.H. Cutler, J. Phys. Chem., B 102 (1998) 4165.
[20] J.S. Lee, G.H. Gu, H. Kim, K.S. Jeong, J. Bae, J.S. Suh, Chem. Mater. 13 (2001) 2387.
[21] K.B.K. Teo, D.B. Hash, R.G. Larcerda, N.L. Rupesinghe, M.S. Bell, S.H. Dalal, D. Bose, T.R. Govindan, B.A. Cruden, M. Chhowalla, G.A.J. Amaratuga, M. Meyyappan, W.I. Milne, Nano Lett. 4 (2004) 921.
[22] J.E. Sader, J.W.M. Chon, P. Mulvaney, Rev. Sci. Instrum. 70 (1999) 3967.
[23] R.S. Lakes, T. Lee, A. Bersie, Y.C. Wang, Nature 410 (2001) 565.
[24] R.S. Lakes, Philos. Mag. Lett. 81 (2001) 95.
[25] H.W. Yap, R.S. Lakes, R.W Carpick, in preparation.